A Global Pattern of Thermal Adaptation in Marine Phytoplankton

Mridul K. Thomas *et al.*

Science **338**, 1085 (2012);
DOI: 10.1126/science.1224836

A Global Pattern of Thermal Adaptation in Marine Phytoplankton

Mridul K. Thomas,[1,2]*† Colin T. Kremer,[1,3]† Christopher A. Klausmeier,[1,3] Elena Litchman[1,2]

Rising ocean temperatures will alter the productivity and composition of marine phytoplankton communities, thereby affecting global biogeochemical cycles. Predicting the effects of future ocean warming on biogeochemical cycles depends critically on understanding how existing global temperature variation affects phytoplankton. Here we show that variation in phytoplankton temperature optima over 150 degrees of latitude is well explained by a gradient in mean ocean temperature. An eco-evolutionary model predicts a similar relationship, suggesting that this pattern is the result of evolutionary adaptation. Using mechanistic species distribution models, we find that rising temperatures this century will cause poleward shifts in species' thermal niches and a sharp decline in tropical phytoplankton diversity in the absence of an evolutionary response.

Marine phytoplankton are responsible for nearly half of global primary productivity (*1*). They play essential roles in food webs and global cycles of carbon, nitrogen, phosphorus, and other elements (*2*, *3*). Empirical studies have shown that recent ocean warming has driven changes in productivity (*4*), population size (*5*), phenology (*6*), and community composition (*7*). Global ocean circulation models predict further temperature-driven reductions in phytoplankton productivity this century, with consequent decreases in marine carbon sequestration (*8*, *9*). The main mechanism that these studies have identified is indirect: Rising temperatures drive an increase in ocean stratification, which in turn leads to a decrease in nutrient supply to surface waters. However, most models do not consider the direct effects of rising temperatures on individual phytoplankton species, which experience sharp declines in growth rate above their optimum temperatures for growth. They may, therefore, underestimate the effects of warming on ecosystems.

To understand how ocean warming will directly affect marine and estuarine phytoplankton, we examined growth responses to temperature in 194 strains belonging to more than 130 species from the major phytoplankton groups (*10*). Temperature-related traits, such as the optimum temperature for growth and the thermal niche width (the temperature range over which growth rate is positive), are among the most important in ectothermic species, especially given predictions of global warming (*11*). We estimated these traits from >5000 growth rate measurements, synthesized from 81 papers published between 1935 and 2011. The strains were isolated from 76°N to 75°S, giving us exceptionally broad coverage of the latitudinal and temperature gradients (fig. S1).

Growth responses to changes in temperature are characterized by thermal tolerance curves (reaction norms). Two features of these curves are common to all ectotherms: unimodality and negative skewness (i.e., a sharper decline in fitness above the optimum temperature than below) (fig. S2) (*11*, *12*). The latter condition makes ectotherms living at their optimum temperature more sensitive to warming than cooling, with important consequences for their performance in the environment (*13*). Furthermore, there is an exponential increase in the maximum growth rate attainable with increasing temperature (across species). These curves may be described using three principal traits: maximum growth rate, optimum temperature for growth, and thermal niche width. We estimated these traits for each strain by fitting a thermal tolerance function to the data (*14*) and examined their relationships with environmental and taxonomic covariates (*10*).

Our analysis revealed large-scale patterns in thermal traits. First, strains exhibited a clear latitudinal trend in the optimum temperature for growth [Fig. 1, coefficient of determination (R^2) = 0.55, $P < 0.0001$], demonstrating the existence of a global pattern in a key microbial trait. Second, optimum temperature was even more strongly related to mean annual temperature at the isolation location (Fig. 2A, $R^2 = 0.69$, $P < 0.0001$), suggesting that temperature is a major selective agent and that adaptation to local environmental conditions occurs in marine microbes despite the potential for long-distance dispersal through ocean currents. In contrast, the width of the thermal niche was unrelated to temperature regimes. Third, strains from polar and temperate waters had optimum temperatures that were considerably higher than their mean annual temperatures, whereas tropical strains had optima closer to or lower than the mean temperatures (Fig. 2A). Finally, variation in optimum temperature and niche width was not explained by taxonomic differences above the level of genus, indicating that thermal adaptation is not highly phylogenetically constrained in this group (tables S1 and S2).

This strong trait-environment relationship suggests that microbes are adapted to the temperatures that they experience locally. However, this pattern could also occur through a correlated response to selection on other traits. To test whether the observed pattern arose as an adaptive response to variable thermal regimes, we used an eco-evolutionary model (*15*, *16*) to predict the optimum temperatures that maximize fitness at each isolation location. The model allows us to study the effects of thermal adaptation alone by forcing all other aspects of strains to be identical. Purely theoretical applications of such eco-evolutionary models have been extensive, but they have rarely been compared to quantitative field data (*17*).

In the model, strains differ only in their thermal tolerance curves (characterized by their optimum temperature) while competing for a single

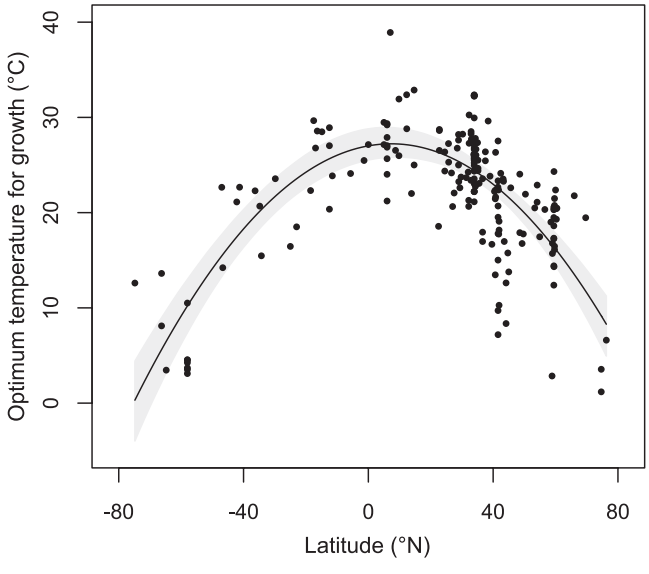

Fig. 1. Latitudinal gradient in the optimum temperature for growth of marine and estuarine phytoplankton strains (n = 194 strains, R^2 = 0.55, $P < 0.0001$). Each point represents the optimum temperature for growth of a single strain, estimated by fitting a thermal tolerance function (*14*) to the data. The regression line (black) is shown, along with 95% confidence bands (gray). Confidence bands account for asymmetric uncertainty in trait estimates using a bootstrapping algorithm [(*10*), see also fig. S9].

[1]W. K. Kellogg Biological Station, Michigan State University, Hickory Corners, MI 49060, USA. [2]Department of Zoology, Michigan State University, East Lansing, MI 48824, USA. [3]Department of Plant Biology, Michigan State University, East Lansing, MI 48824, USA.

*To whom correspondence should be addressed. E-mail: thomasmr@msu.edu

†These authors contributed equally to this work.

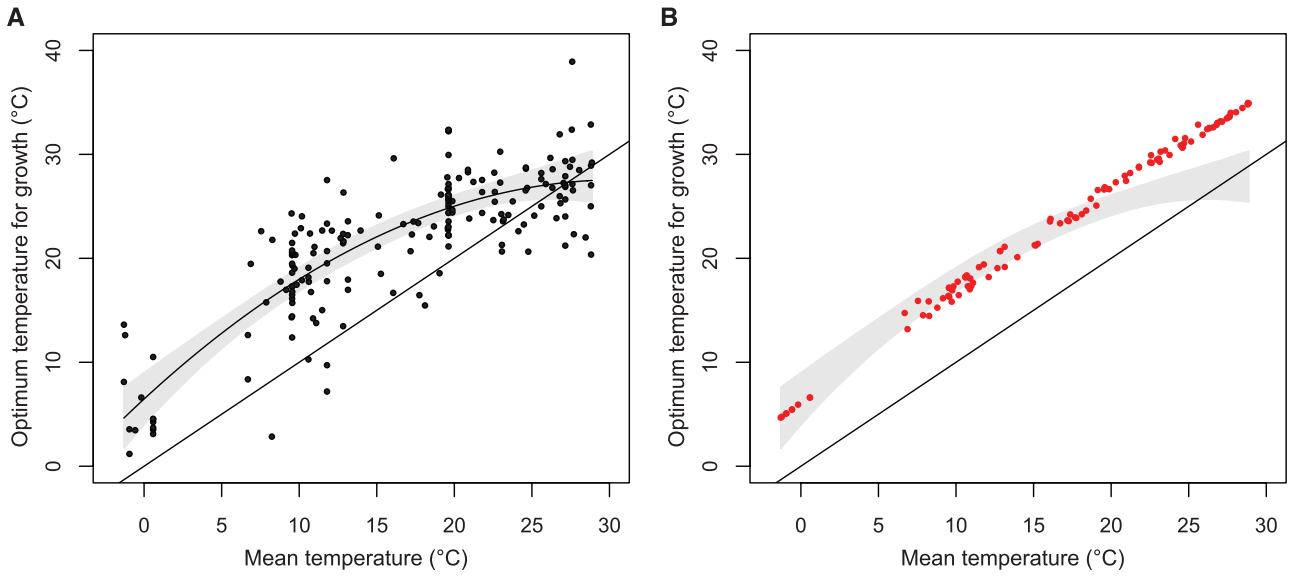

Fig. 2. Optimum temperatures for growth across a gradient of ocean temperature. (**A**) The optimum temperature of phytoplankton strains is well explained by variation in the mean annual temperature at their isolation locations ($n = 194$, $R^2 = 0.69$, $P < 0.0001$), indicating adaptation to local environmental conditions. The 1:1 line (black, straight), regression line (black, curved) and 95% confidence bands (gray) from bootstrapping are shown (*10*). The regression line shown is for the best model (table S4), which posits a quadratic relationship between mean temperature and optimum temperatures. (**B**) The eco-evolutionary model predicts evolutionarily stable optimum temperatures (red points) for each isolation location that are several degrees higher than the mean environmental temperatures (i.e., above the black line) and agree well with the data, except in the warmest waters. The confidence band from (A) is shown in gray for comparison.

nutrient. The growth rates of all strains are bounded by an exponential function that increases with temperature, an empirical relationship known as the Eppley curve (*12*). We require that each individual strain's thermal tolerance curve touch the Eppley curve at a single point, forcing maximum growth rate to become a function of optimum temperature. Niche widths are held constant across strains, because we found no significant relationship in our data set between niche width and environmental or taxonomic covariates (tables S1 and S2). Given these constraints, we allow optimum temperatures of a set of strains to evolve in response to deterministic temperature regimes. These regimes were based on model fits to a 30-year sea surface temperature time series at every isolation location (*10*, *18*). For each environment, we used an evolutionary algorithm based on quantitative genetics to identify evolutionarily stable states (ESSs) (*10*, *16*). At an ESS, the strains that persist (defined by their traits) cannot be invaded by any other strain. These temperature optima serve as a theoretical prediction of the best strategy (or strategies) at each isolation location, which we can then compare to our data as a test of thermal adaptation.

Our eco-evolutionary model predicts that optimum temperatures should increase with mean temperature and exceed it by several degrees (Fig. 2B and fig. S3). This is in agreement with the observed pattern (Fig. 2A) and bolsters the case that this relationship arises from adaptation to mean temperature. However, in regions with the highest mean temperatures (the tropics), the model predicts optima that are significantly higher than those observed. Although this discrepancy suggests that tropical strains may be less well-adapted to their environmental temperatures, we estimated that these strains are capable of persistence under the temperature regimes they experience (Figs. 2B and 3) (*19*). The difference may be a result of interactions between temperature and other factors, constraints on thermal adaptation at high temperatures, or adaptation to laboratory temperatures before measurement. Examining model predictions across a range of assumed niche widths reveals that wider niches lead to larger differences between predicted optima and the mean annual temperatures and to a decrease in the number of coexisting strains (fig. S3). These results illustrate that temperature variation can support species coexistence, although it cannot fully explain the levels of trait diversity observed in the data.

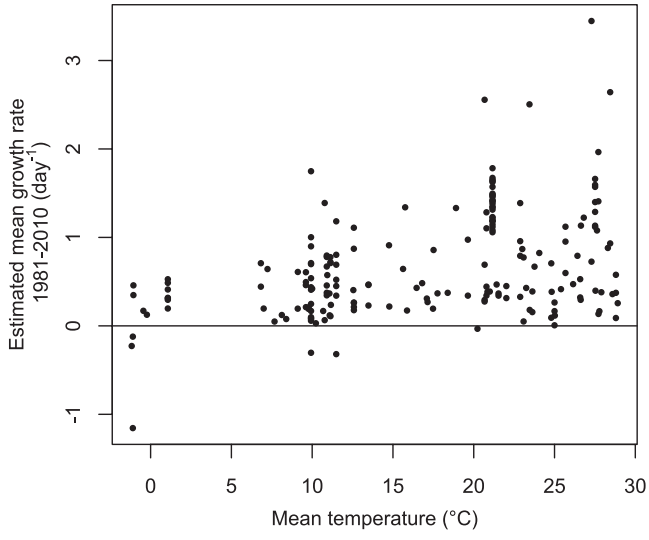

Fig. 3. Estimated mean daily growth rates of all strains at their isolation locations, between 1980 and 2010. These estimates were based on monthly temperature records (*19*) and each strain's thermal tolerance curve, and depend on the assumption that growth is limited solely by temperature. Even warm-water strains have mean growth rates exceeding zero (the horizontal line), indicating that they are capable of persisting in their environment, although their optima are below what our model predicts to be most adaptive.

Phytoplankton strains may be adapted to their current conditions, but could be negatively affected by warming oceans. Moving from the eco-evolutionary model to purely physiological mechanistic species distribution models (SDMs), we then examined whether changing environmental temperatures could alter species ranges and global diversity patterns. These models use physiological trait measurements to predict species abundances across environmental gradients (*20*) but do not account for species interactions or

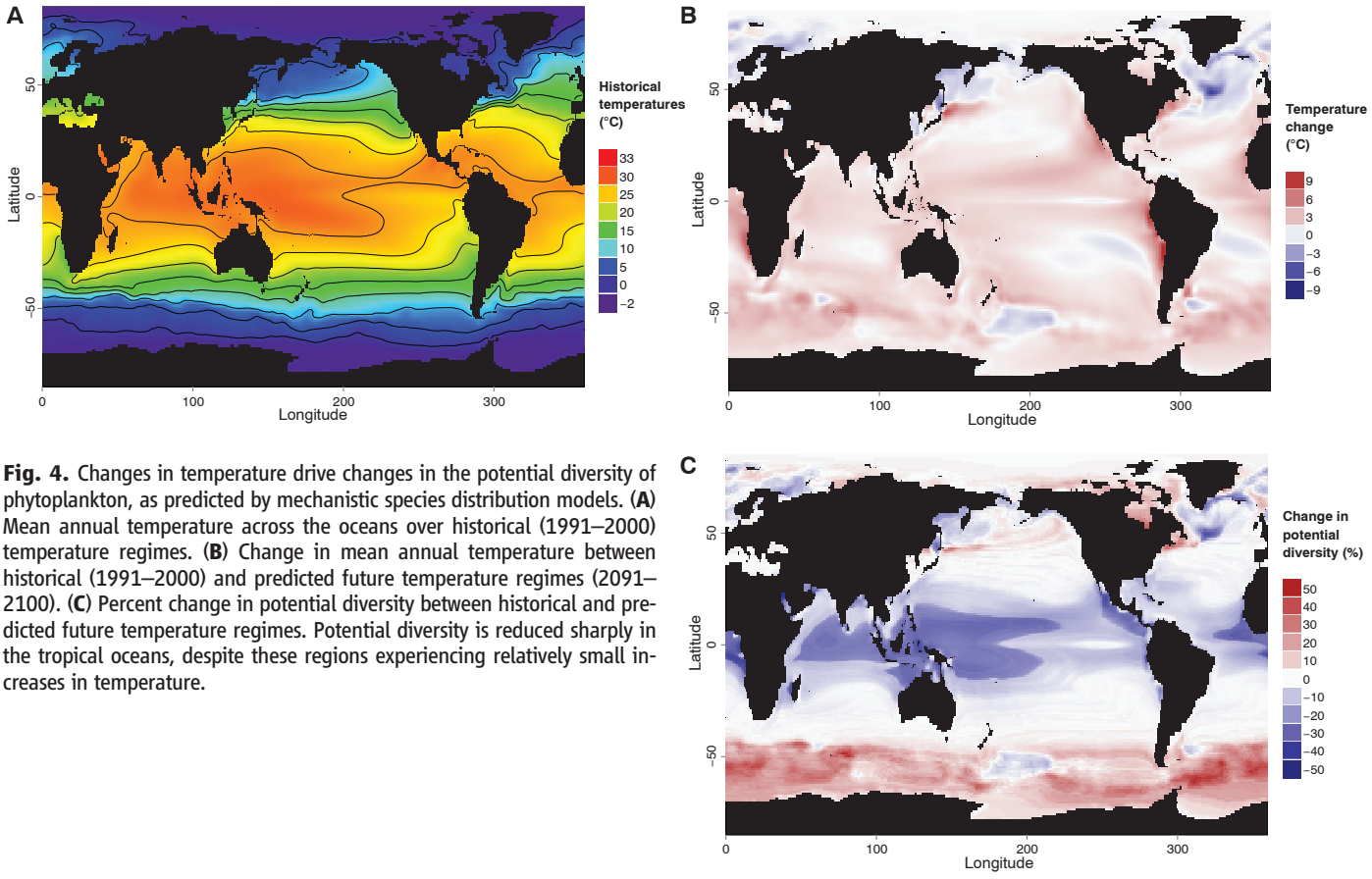

Fig. 4. Changes in temperature drive changes in the potential diversity of phytoplankton, as predicted by mechanistic species distribution models. (**A**) Mean annual temperature across the oceans over historical (1991–2000) temperature regimes. (**B**) Change in mean annual temperature between historical (1991–2000) and predicted future temperature regimes (2091–2100). (**C**) Percent change in potential diversity between historical and predicted future temperature regimes. Potential diversity is reduced sharply in the tropical oceans, despite these regions experiencing relatively small increases in temperature.

evolution. We generated growth rate predictions across the ocean for each strain represented in our data set, based on their thermal tolerance curves and a 10-year temperature time series (*10*). If the 10-year mean growth rate of a strain was positive at a location, the location was deemed to fall within its range. We repeated this using both historical (1991–2000) and future (2091–2100) temperature regimes, the latter having been predicted by a global climate model (*10*, *19*, *21*–*23*). These estimates indicate that ocean warming is likely to drive poleward shifts in strains' equatorial boundaries, although polar range boundaries remain approximately constant (fig. S4). Consequently, many strains are predicted to experience a reduction in range size (figs. S5, S6, and S12), potentially increasing extinction probabilities. Our SDMs assume that growth rates are limited solely by temperature, but other factors, such as nutrient availability, could also be incorporated if relevant trait data were available.

When the range shifts of all strains are considered in the aggregate, they can be used to predict global patterns of phytoplankton diversity change as a result of ocean warming (Fig. 4) (*24*). In order to do this, we calculated "potential diversity," defined as the number of phytoplankton strains (out of the 194 in our data set) theoretically capable of growing at a location, assuming that temperature is the sole limiting factor (figs. S7 and S8). A comparison of potential diversity patterns under both historical and future temperature regimes shows that temperature change may drive a large reduction in tropical phytoplankton diversity over the course of this century. Approximately one-third of contemporary tropical strains are unlikely to persist there in 2100 (Fig. 4C), despite a change in mean temperature of only ~2°C (Fig. 4, A and B). High latitudes may experience small increases in potential diversity, as a result of poleward shifts in strain ranges. Rising temperatures have the strongest effect on tropical strains, because tropical optima are close to current mean temperatures (Fig. 2A) and thermal tolerance curves are negatively skewed. Small increases in temperature can therefore lead to sharp declines in growth rate. A decrease in diversity is likely to have a strong impact on tropical ecosystems, because biodiversity loss is a major cause of ecosystem change (*25*). One possible consequence is a decrease in tropical primary productivity, which could occur through two distinct mechanisms: the loss of highly productive species or a decrease in complementarity (*26*, *27*).

Our findings lend support to the hypothesis that tropical communities are most vulnerable to increases in temperature (*28*). However, the existence of high genetic diversity within species, as has been noted in some cases (*29*), may prevent the loss of entire species. Adaptation to changing temperatures may mitigate some of the predicted losses in diversity, particularly in rapidly reproducing taxa such as phytoplankton. The evolution of thermal tolerance has been examined in a few taxa, including phytoplankton (*30*–*32*), but we currently lack the information necessary to accurately model the consequences of evolutionary change on ecosystem processes (*33*, *34*). In the case of phytoplankton, we need estimates of rates of adaptation to high temperature stress in a variety of taxa, as well as an examination of the evolutionary constraints and trade-offs that may be associated with this. Characterizing these constraints will allow us to make improved forecasts of species survival and may prove critical for understanding the fate of tropical communities and oceanic ecosystems.

References and Notes

1. C. B. Field, M. J. Behrenfeld, J. T. Randerson, P. G. Falkowski, *Science* **281**, 237 (1998).
2. A. C. Redfield, *Am. Sci.* **46**, 205 (1958).
3. P. G. Falkowski, R. T. Barber, V. Smetacek, *Science* **281**, 200 (1998).
4. M. J. Behrenfeld *et al.*, *Nature* **444**, 752 (2006).
5. D. G. Boyce, M. R. Lewis, B. Worm, *Nature* **466**, 591 (2010).
6. M. Edwards, A. J. Richardson, *Nature* **430**, 881 (2004).
7. X. A. G. Morán, Á. López-Urrutia, A. Calvo-Díaz, W. K. W. Li, *Glob. Change Biol.* **16**, 1137 (2010).
8. L. Bopp *et al.*, *Global Biogeochem. Cycles* **15**, 81 (2001).
9. M. Steinacher *et al.*, *Biogeosciences* **7**, 979 (2010).
10. Materials and methods are available as supplementary materials on *Science* Online.

11. J. G. Kingsolver, *Am. Nat.* **174**, 755 (2009).
12. R. W. Eppley, *Fish Bull.* **70**, 1063 (1972).
13. T. L. Martin, R. B. Huey, *Am. Nat.* **171**, E102 (2008).
14. J. Norberg, *Limnol. Oceanogr.* **49**, 1269 (2004).
15. S. A. H. Geritz, É. Kisdi, G. Meszéna, J. A. J. Metz, *Evol. Ecol.* **12**, 35 (1997).
16. P. A. Abrams, *Ecol. Lett.* **4**, 166 (2001).
17. J. C. Stegen, R. Ferriere, B. J. Enquist, *Proc. Biol. Sci.* **279**, 1051 (2011).
18. R. W. Reynolds *et al.*, *J. Clim.* **20**, 5473 (2007).
19. R. W. Reynolds, N. A. Rayner, T. M. Smith, D. C. Stokes, W. Wang, *J. Clim.* **15**, 1609 (2002).
20. M. R. Kearney, W. Porter, *Ecol. Lett.* **12**, 334 (2009).
21. Intergovernmental Panel on Climate Change (IPCC), *Climate Change 2007: The Physical Science Basis. Contribution of Working Group I to the Fourth Assessment Report of the Intergovernmental Panel on Climate Change*, S. Solomon *et al.*, Eds. (Cambridge Univ. Press, Cambridge, 2007).
22. N. Nakićenović *et al.*, *Special Report on Emissions Scenarios: A Special Report of Working Group III of the Intergovernmental Panel on Climate Change*, N. Nakićenović, R. Swart, Eds. (Cambridge Univ. Press, Cambridge, 2000); www.osti.gov/energycitations/product.biblio.jsp?osti_id=15009867.
23. T. Delworth *et al.*, *J. Clim.* **19**, 643 (2006).
24. D. W. McKenney, J. H. Pedlar, K. Lawrence, K. Campbell, M. F. Hutchinson, *Bioscience* **57**, 939 (2007).
25. D. U. Hooper *et al.*, *Nature* **486**, 105 (2012).
26. D. Tilman, D. Wedin, J. Knops, *Nature* **379**, 718 (1996).
27. P. B. Reich *et al.*, *Science* **336**, 589 (2012).
28. C. A. Deutsch *et al.*, *Proc. Natl. Acad. Sci. U.S.A.* **105**, 6668 (2008).
29. K. Härnström, M. Ellegaard, T. J. Andersen, A. Godhe, *Proc. Natl. Acad. Sci. U.S.A.* **108**, 4252 (2011).
30. A. F. Bennett, R. E. Lenski, in *In the Light of Evolution. Volume 1. Adaptation and Complex Design*, J. C. Avise, F. J. Ayala, Eds. (National Academies Press, Washington, DC, 2007), pp. 225–238.
31. J. L. Knies, R. Izem, K. L. Supler, J. G. Kingsolver, C. L. Burch, *PLoS Biol.* **4**, e201 (2006).
32. I. E. Huertas, M. Rouco, V. López-Rodas, E. Costas, *Proc. Biol. Sci.* **278**, 3534 (2011).
33. S. L. Chown *et al.*, *Clim. Res.* **43**, 3 (2010).
34. M. J. Angilletta Jr., R. S. Wilson, C. A. Navas, R. S. James, *Trends Ecol. Evol.* **18**, 234 (2003).

Acknowledgments: This research was supported by NSF (grants DEB-0845932, DEB-0845825, and OCE-0928819), including the BEACON Center for the Study of Evolution in Action (grant DBI-0939454) and a Graduate Research Fellowship to C.T.K., as well as a grant from the James S. McDonnell Foundation. K. Edwards and N. Swenson provided statistical advice, and J. Lennon, G. Mittelbach, and E . Miller provided comments on the manuscript. The trait data presented are shown in table S5, and the collated growth rate data are in table S6. Also thanks to NOAA/OAR/ESRL PSD, Boulder, CO, USA, for NOAA_OI_SST_V2 data provided at their Web site, www.esrl.noaa.gov/psd/. This is W. K. Kellogg Biological Station contribution number 1694. E.L. and M.K.T. conceived the original idea; M.K.T. collected the growth-temperature data; M.K.T. and C.T.K. analyzed the data; C.T.K. and C.A.K. developed and C.T.K. analyzed the eco-evolutionary model; M.K.T. and C.T.K. ran the mechanistic species distribution models; and M.K.T., C.T.K., and E.L. wrote and C.A.K. commented on the manuscript.

Supplementary Materials

www.sciencemag.org/cgi/content/full/science.1224836/DC1
Materials and Methods
Figs. S1 to S12
Tables S1 to S6
References (*35*–*135*)

17 May 2012; accepted 10 October 2012
Published online 25 October 2012;
10.1126/science.1224836

Decoding Human Cytomegalovirus

Noam Stern-Ginossar,[1] Ben Weisburd,[1] Annette Michalski,[2]* Vu Thuy Khanh Le,[3] Marco Y. Hein,[2] Sheng-Xiong Huang,[4] Ming Ma,[4] Ben Shen,[4,5,6] Shu-Bing Qian,[7] Hartmut Hengel,[3] Matthias Mann,[2] Nicholas T. Ingolia,[1]† Jonathan S. Weissman[1]*

The human cytomegalovirus (HCMV) genome was sequenced 20 years ago. However, like those of other complex viruses, our understanding of its protein coding potential is far from complete. We used ribosome profiling and transcript analysis to experimentally define the HCMV translation products and follow their temporal expression. We identified hundreds of previously unidentified open reading frames and confirmed a fraction by means of mass spectrometry. We found that regulated use of alternative transcript start sites plays a broad role in enabling tight temporal control of HCMV protein expression and allowing multiple distinct polypeptides to be generated from a single genomic locus. Our results reveal an unanticipated complexity to the HCMV coding capacity and illustrate the role of regulated changes in transcript start sites in generating this complexity.

The herpesvirus human cytomegalovirus (HCMV) infects the majority of humanity, leading to severe disease in newborns and immunocompromised adults (*1*). The HCMV genome is ~240 kb with estimates of between 165 and 252 open reading frames (ORFs) (*2*, *3*). These annotations likely do not capture the complexity of the HCMV proteome (*4*) because HCMV has a complex transcriptome (*5*, *6*), and genomic regions studied in detail reveal noncanonical translational events, including regulatory (*7*) and overlapping ORFs (*8*–*11*). Defining the full set of translation products—both stable and unstable, the latter with potential regulatory/antigenic function (*12*)—is critical for understanding HCMV.

To identify the range of HCMV-translated ORFs and monitor their temporal expression, we infected human foreskin fibroblasts (HFFs) with the clinical HCMV strain Merlin and harvested cells at 5, 24, and 72 hours after infection using four approaches to generate libraries of ribosome-protected mRNA fragments (Fig. 1A and table S1). The first two measured the overall in vivo distribution of ribosomes on a given message; infected cells were either pretreated with the translation elongation inhibitor cycloheximide or, to exclude drug artifacts, lysed without drug pretreatment (no-drug). Additionally, cells were pretreated with harringtonine or lactimidomycin (LTM), two drugs with distinct mechanisms, which lead to strong accumulation of ribosomes at translation initiation sites and depletion of ribosomes over the body of the message (Fig. 1A) (*13*–*15*). A modified RNA sequencing protocol allowed quantification of RNA levels as well as identification of 5′ transcript ends by generating a strong overrepresentation of fragments that start at the 5′ end of messages (fig. S1) (*16*).

The ability of these approaches to provide a comprehensive view of gene organization is illustrated for the UL25 ORF: A single transcript start site is found upstream of the ORF (Fig. 1A, mRNA panel). Harringtonine and LTM mark a single translation initiation site at the first AUG downstream of the transcript start (Fig. 1A, Harr and LTM). Ribosome density accumulates over the ORF body ending at the first in-frame stop codon (Fig. 1A, CHX and no-drug). In the no-drug sample, excess ribosome density accumulates at the stop codon (Fig. 1A, no-drug) (*14*).

Examination of the full range of HCMV translation products, as reflected by the ribosome footprints, revealed many putative previously unidentified ORFs: internal ORFs lying within existing ORFs either in-frame, resulting in N-terminally truncated translation products (Fig. 1B), or out of frame, resulting in entirely previously unknown polypeptides (Fig. 1C); short uORFs (upstream ORFs) lying upstream of canonical ORFs (Fig. 2A); ORFs within transcripts antisense to canonical ORFs (Fig. 2B); and previously unidentified short ORFs encoded by distinct transcripts (Fig. 2C). For all of these categories, we also observed ORFs starting at near-cognate codons (codons differing from AUG by one nucleotide), especially CUG (Fig. 2D).

HCMV expresses several long RNAs lacking canonical ORFs, including β2.7, an abundant RNA, which inhibits apoptosis (*17*). In agreement with β2.7's observed polysome association (*18*), multiple short ORFs are translated from this RNA (Fig. 2E and fig. S2), and the corresponding proteins for two of these ORFs were detected by means of high-resolution MS (Fig. 2E). Although the translation efficiency

[1]Department of Cellular and Molecular Pharmacology, Howard Hughes Medical Institute, University of California, San Francisco, San Francisco, CA 94158, USA. [2]Department of Proteomics and Signal Transduction, Max Planck Institute of Biochemistry, Martinsried D-82152, Germany. [3]Institut für Virologie, Heinrich-Heine-Universität Düsseldorf, 40225 Düsseldorf, Germany. [4]Department of Chemistry, Scripps Research Institute, 130 Scripps Way #3A2, Jupiter, FL 33458, USA. [5]Department of Molecular Therapeutics, Scripps Research Institute, 130 Scripps Way #3A2, Jupiter, FL 33458, USA. [6]Natural Products Library Initiative at The Scripps Research Institute, Scripps Research Institute, 130 Scripps Way #3A2, Jupiter, FL 33458, USA. [7]Division of Nutritional Sciences, Cornell University, Ithaca, NY 14853, USA.

*To whom correspondence should be addressed. E-mail: michalsk@biochem.mpg.de (A.M.); weissman@cmp.ucsf.edu (J.S.W.)

†Present address: Department of Embryology, Carnegie Institute for Science, Baltimore, MD 21218, USA.